Chemical vapor deposition of Pd/Cu alloy films from a new single source precursor

Vladislav V. Krisyuk [a,*], Yuriy V. Shubin [a,c], François Senocq [b], Asiya E. Turgambaeva [a], Thomas Duguet [b], Igor K. Igumenov [a], Constantin Vahlas [b]

[a] Nikolaev Institute of Inorganic Chemistry SB RAS, Pr. Acad. Lavrentiev 3, Novosibirsk 630090, Russia
[b] CIRIMAT, ENSIACET, 4, allée Emile Monso, BP-44362, 31030 Toulouse Cedex 4, France
[c] Novosibirsk State University, 2, Pirogova Str., Novosibirsk 630090, Russia

Keywords:
A3. Metalorganic chemical vapor deposition
A3. Polycrystalline deposition
B1. Metals
B3 Pd-alloy membranes

A B S T R A C T

Cu/Pd alloys were deposited onto Si(100) and SiO_2 (fused silica) substrates by MOCVD from $PdL_2 \times CuL_2$, (L=2-methoxy-2,6,6-trimethylheptane-3,5-dionate), a new single source bimetallic precursor. Deposition was performed at 10 Torr in a temperature range between 200 °C and 350 °C and was assisted by vacuum ultraviolet (VUV) irradiation of the precursor vapor from an excimer Xe-lamp. It was shown that the elemental and phase composition of the films can be controlled by varying the deposition temperature and by stimulating by VUV the precursor decomposition. The bulk compositional properties of the obtained films confirmed the feasibility of proposed approach and precursor to prepare Pd alloy membrane materials by the CVD method.

1. Introduction

The increased demand for hydrogen in recent years has revived the interest in methods for separation and purification of hydrogen from gas mixtures in many sectors such as petroleum refining, petrochemical and semiconductor processing, as well as in new energy-related applications, especially in clean fuel for fuel cells and vehicles. Efficient hydrogen separation membrane alloys are characterized by high hydrogen permeability, low expansion when saturated with hydrogen, good corrosion resistance and high plasticity and strength during operation at temperatures in the range between 300 °C and 700 °C. The main concerns with membrane reliability are related to corrosion resistance and to structural modifications during operation resulting in change of hydrogen permeability. Pd alloy membranes with high selectivity for hydrogen and convenient thermal, chemical, and mechanical properties are widely used for this purpose [1]. Pd–Cu membranes are cost effective materials and have high resistance to sulfurous compounds in gas mixtures while maintaining a desirable set of properties [2–11]. It has been established that $Pd_{47}Cu_{53}$ with B2 (*bcc*) structure shows higher permeability than Pd at 350 °C; the Pd–Cu B2 phase is not thermally stable and is subject to surface poisoning while *fcc* Pd–Cu alloys show some resistance to surface poisoning. Pd–Cu membranes exhibit better performance than Pd-sputtered membranes at high current densities in direct alcohol fuel cells as a primary power source for stationary and portable devices [12–15]. In a complementary perspective, electromigration resistant Pd/Cu alloy films have also been investigated in microelectronics as conductive or buffer layers in circuit design [16,17].

Up to now, many deposition techniques have been investigated to fabricate Pd–Cu composite films. However, to the best of the authors knowledge, there is actually no industrially implemented method of obtaining Pd membranes, each one having its problems yet unsolved. For example, wet deposition techniques like electroless and electro deposition are less suitable for the production of binary, ternary and multicomponent Pd-alloys due to difficulties in controlling the alloy composition and layer thickness on large areas. Processing of Pd–Cu and, more generally of intermetallic alloy coatings by metal organic chemical vapor deposition (MOCVD) is expected to extend their implementation in surface engineering. Especially, thanks to the possibility to operate in surface reaction controlled regime, MOCVD allows surface treatment of complex-in-shape items such as glass molds, turbine blades and vanes in aeronautic industries, or porous preforms whose internal surface may be functionalized for the preparation of supported catalysts. High growth rate, versatility, cost effectiveness, environmental compatibility, ease to scale up and the possibility to process films containing thermodynamically metastable phases, are additional advantages of MOCVD processes. Finally, the use of molecular precursors allows operating at low to moderate temperatures, thus extending the targeted applications spectrum so as to cover temperature-sensitive substrates.

* Corresponding author.
E-mail address: kvv@niic.nsc.ru (V.V. Krisyuk).

http://dx.doi.org/10.1016/j.jcrysgro.2014.09.032

The price to pay for this high potential is the need to tackle the challenges imposed by the complex gas phase and surface chemistries. In addition to mastering the deposition reaction, these challenges also concern the precursor design and delivery, in terms of non-toxicity, stability and volatility. The inherent difficulty for the establishment of a robust MOCVD process is further amplified in the case of coatings containing several elements and potentially intermetallic phases, mainly because of the limited width of their stability domains, the far-from-equilibrium initial state which can lead to unpredicted transitions and, last but not the least, of the requirement to use compatible precursors for the deposited elements [18]. Until now, this situation resulted in limited investigation of MOCVD for the co-deposition of intermetallic alloy films. The above mentioned constraints can be partially circumvented if the preparation of the coating proceeds through the use of a single source precursor. In the case of Pd–Cu based membranes, it would be useful to dispose of a precursor providing deposition of the base Pd–Cu alloy when another component (e.g. Ag, Ru, V, Y, Zr, etc.) which is of minor content (several at%) can be codeposited from the separate compound.

In this perspective, the present contribution is focused on the investigation of $PdL_2 \times CuL_2$, (L=2-methoxy-2,6,6-trimethylheptane-3,5-dionate), an original single source, volatile precursor with a Pd/Cu ratio equal to one, for the CVD of Pd–Cu films. CVD of Pd–Cu films is performed under thermal activation. Moreover, vacuum ultraviolet activation of the input gas is combined with thermal activation with the aim to improve the film quality and/or to decrease the thermal budget of the process.

2. Experimental

Detailed information on the synthesis and the properties of $[PdL_2 \times CuL_2]$ will be published in the forthcoming paper. It is recalled here that the compound can be sublimed in vacuum (130 °C, 10^{-2} Torr) while preserving its composition and structure.

Pd–Cu films were deposited on Si(100) and fused silica 10×10 mm^2 substrates in a cold wall stainless steel CVD reactor described in Ref. [19]. For each experiment, 30 mg of $[PdL_2 \times CuL_2]$ was conditioned in a glass ampoule; it was sublimed at 130 °C and was transported to the deposition chamber under a flow of 30 standard cubic centimeters (sccm) of Ar. 100 sccm of H_2 was used as a co-reactant. Operating pressure was 10 Torr (1.33×10^3 Pa) and deposition temperature (T_d) was in the range 200–350 °C. VUV stimulation was ensured by a low pressure Xe excimer lamp ($\lambda \sim 172$ nm), produced by CHROMDET Analytical Instruments, (http://www.chromdet.ru). The conversion efficiency of power consumption in the VUV radiation is up to 10%. Generator power ~20 W, working frequency 20–60 kHz and voltage up to 5 kV.

Determination of phases in the films was performed at room temperature by X-ray diffraction in a Shimadzu XRD-7000 instrument (Cu$K\alpha$ radiation, Ni filter, 2θ angle range from 5° to 50°, 2θ step 0.03°). The patterns were recorded in the step-by-step mode in the angular range 2θ=25–105°, step 0.05°. Data from the PDF database were used as Ref. [20]. The crystal cell parameters were determined by the full profile technique applied to full-range diffraction data using the PowderCell 2.4 software [21]. The volume-averaged crystallite sizes (D) were estimated from the integral broadening of the peaks using the WINFIT 1.2.1 program and the Scherrer formula [22]. The composition of the Cu_xPd_{1-x} bimetallic phases was determined from the specific atomic volumes ($\nu n = V_{cel}/z_{at}$) by using a calibration curve built from crystal cell parameters of known alloys [20]. The significant difference in the specific atomic volumes of the elements (νn_{Cu}=11.81, νn_{Pd}=14.72 Å^3) allowed determination of the alloys composition with ±1 at% precision. The weight ratio of the phases in the films was approximated by the ratio of the integral intensities of the reflections (110) for phase B2 and (111) for phase *fcc*, with an adjustment factor obtained from corundum numbers (RIR): $k(B2) = I_{110}/I_c = 16.15$ (PDFcard 01-071-7806), $k(fcc) = I_{111}/I_c = 12.62$ (PDFcard 01-071-7806); $m_{B2}(\%) = I_{110} \times k(fcc)/(I_{110} \times k(fcc) + I_{111} \times k(B2))100\%$. The relative error of the determination is not more than 10%.

Films morphology was investigated by scanning electron microscopy (SEM) with a JEOL JSM 6700F instrument equipped with a JEOL EX-23000 BU energy-dispersive X-ray spectrometer (EDS) analyzer. Surface composition was investigated by X-ray photoelectron spectroscopy (XPS) with a VG ESCALAB HP instrument using Al $K\alpha$ ($h\nu n$=1486.6 eV) non-monochromatic radiation. The samples were mounted on a sample holder using double side adhesive, conductive tape. The calibration of the scale of binding energies was done on the Au4$f_{7/2}$ (E_B=84.0 eV) and Cu2$p_{3/2}$ (E=932.9 eV) lines from Au and Cu foils, respectively. The spectra were recorded before and after sputtering with a focused Ar^+ ion beam with energy of 3 keV at a current density of *ca.* 40 μA/cm^2. The relative concentrations of the elements were determined on the basis of the integrated intensities of XPS lines taking into account the photoionization cross sections of the corresponding terms [23].

The elemental composition of the films was also determined by Electron Probe Micro-Analysis (EPMA) with a CAMECA SX-50 instrument, equipped with three wavelength dispersive spectrometers, and by inductively-coupled plasma atomic emission spectroscopy (ICP-AES) with a Thermo Scientific ICAP-6500 instrument. Films deposited on fused silica substrates were investigated for the latter case. Prior to the analysis the films were dissolved in nitric acid and the obtained solutions were subjected to a standard analytical protocol.

3. Results and discussion

Film formation was observed on quartz and silicon substrates and also on the stainless steel susceptor. Films deposited both on silicon and quartz substrates are mirror like and present a gray metallic gloss. The mass gain per unit surface of SiO_2 samples was typically ~1.5 times higher than that of the Si ones at all T_d. No film formation was observed at T_d lower than 150 °C for deposition time of 1 h, even under VUV-irradiation. These results are attributed to a higher nucleation delay of the film at low T_d as well as on Si than on SiO_2. This aspect is out of the scope of the present work.

Films were systematically composed of Pd–Cu crystalline phases with different Pd/Cu ratio depending on T_d. The Cu–Pd phase diagram contains two solid solutions; a disordered *fcc* (space group Fm-3m) which spans over the entire compositional range, and a *bcc* intermetallic CuPb or B2 phase (CsCl structure, space group Pm−3m), stable up to *ca.* 600 °C [24–26]. The latter appears in the form of a miscibility gap centered on 40 at% Pd and expanding from 30 at% to 50 at% at room temperature. The two diagrams of Fig. 1 present XRD patterns of films deposited at different temperatures on SiO_2, under thermal (1a) and combined thermal-VUV (1b) activation. Fig. 1 shows that the peaks shift and the lattice parameters change that is good evidence of the alloy film forming. Similar patterns are obtained from films processed on Si. It appears that both the B2 and the *fcc* phases are systematically present in the films. However, the former is largely predominant, in agreement with the thermodynamic equilibria [27]. No crystalline phases of unary metals are detected in the films. Comparison between XRD patterns of films processed with and without VUV activation reveals that the relative amount of the minor *fcc* phase is higher when deposition is VUV activated. This result can be explained by the fact that photostimulation by such a hard radiation results in decomposition of precursor ligands. This in turn produces films with higher carbon contamination as it will be detailed in a following

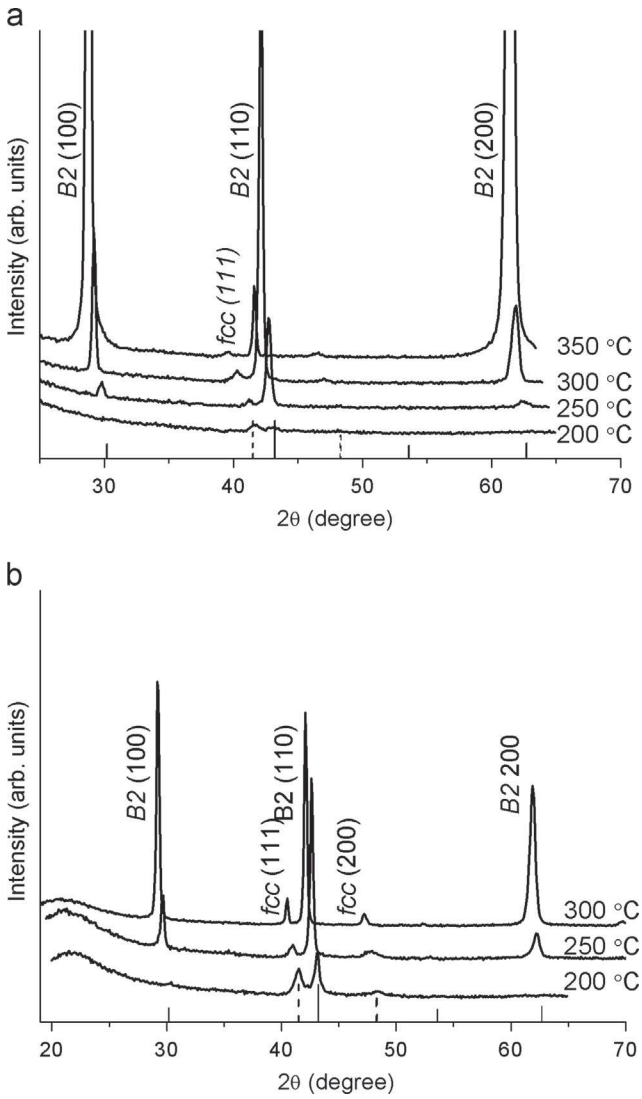

Fig. 1. XRD patterns of Cu–Pd films deposited on SiO_2 films at different T_d under thermal activation (a) and combined thermal and VUV activation (b). Diagrams are incrementally offset by 0.5° with regard to the ones corresponding to T_d=200 °C for clarity. Dot and full vertical lines correspond to the relative main intensities of *fcc* (ICSD card 01-071-7851) and B2 (ICSD card 01-078-4406) phases, respectively.

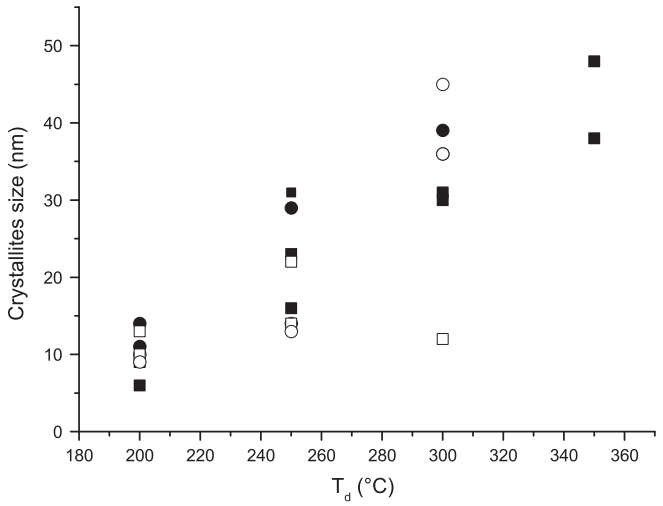

Fig. 2. Crystallites size of the films as a function of T_d. Bold symbols: B2 phase. Open symbols: *fcc* phase. Squares: thermal activation. Circles: combined thermal and VUV activation.

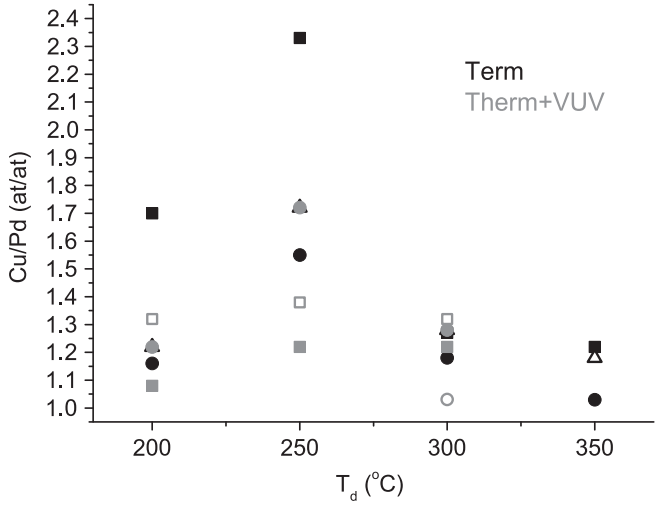

Fig. 3. Cu/Pd atom ratio in the films as a function of T_d. Open and bold symbols correspond to SiO_2 and Si substrates, respectively; squares: EPMA, circles: EDS, triangles: ICP-AES.

section. It is well known that the *fcc* phase is stabilized in the presence of free carbon (see for example [28]).

Films are textured especially those processed at 350 °C which are textured in the ⟨100⟩ direction. Indeed, for these films the intensity of 100 and 200 peaks is match higher than that of the 110 peak, while in films processed at 250 °C, 300 °C and in randomly oriented powder, reflection 110 is the most intense.

From both diagrams 1a and 1b it appears that the increase of the deposition temperature results in the increase of the peaks area and consequently in the increase of the diffracting matter. Assuming that films do not contain any single (Cu, Pd) or alloyed (Cu–Pd) amorphous metallic phases, this trend is attributed to the increase of the growth rate of the films, resulting in an increased final thickness for a given processing time. Fig. 2 presents the evolution of the crystallites size for all samples as a function of T_d. It appears that, low T_d provides films crystallites size equal to 10 ± 5 nm. Increasing T_d results in an almost linear increase of the size of crystallites up to *ca.* 45 nm at 350 °C. It is worth noting that this trend is valid regardless of the substrate (Si, SiO_2) and of the probed phase (B2, *fcc*).

Fig. 3 presents the Cu/Pd atomic ratio in the films as a function of T_d, determined by EPMA, EDS and ICP-AES. It is shown that films are systematically Cu-rich, with a mean value of Cu/Pd ratio at T_d=200 °C equal to 1.36. A slight increase of the Cu/Pd ratio to a mean value of 1.87 is observed at T_d=250 °C before a decrease and stabilization to 1.14 at 350 °C. This general trend is followed by films obtained by both thermally and thermally plus VUV activated processes, with the only difference being a more uniform Cu/Pd profile along T_d, centered at *ca.* 1.22.

The evolution of the Cu/Pd ratio in the films as a function of the distance from the surface was investigated in two samples processed under thermal-VUV activation at 300 °C and at 350 °C, based the area under the Pd3$d_{5/2}$ and Cu2$p_{3/2}$ peaks. For the former sample, the Cu/Pd value is 0.88 at the surface; it slightly increases during the first 2 min of sputtering time to reach a stable value of 1.06. Before ion etching the Cu2$p_{3/2}$ peak position was recorded at 933.2 eV, which is characteristic of Cu^{2+}. Indeed, binding energy of Cu2$p_{3/2}$ in CuO is in the 933.6–934.6 eV range, while in metallic Cu and in Cu_2O it is in the 932.4–932.8 eV range [27,29–34]. The binding energy for Cu2$p_{3/2}$ shifted to 932.2–932.3 eV after ion etching allowing concluding that Cu is in the

metallic state in the film. This was confirmed by the value of the Auger parameter α; i.e. the sum of the binding energy for the Cu2$p_{3/2}$ peak and the Cu*LMM* line on the scale of the kinetic energies of the electrons. In this case there are no "shake-up" satellites and the Auger parameter equals 1851.0 eV which clearly indicates the metallic state of Cu below the film surface. In contrast to Cu, Pd is found in metallic state on the surface. However, in addition to the downwards shift of the Cu2$p_{3/2}$ line, ion etching resulted in a slight increase of the binding energy for Pd3$d_{5/2}$ to 335.5–335.6 eV; i.e. approximately +0.6 eV, compared to the value for pure Pd. This offset can be attributed to the formation of Pd–Cu alloys. Indeed, it has been shown that upon formation of a Ni–Cu alloy the Cu2$p_{3/2}$ and Ni2$p_{3/2}$ lines can be shifted by 0.2 eV and 0.6 eV, respectively [35,36]. Similar results were obtained from the investigation of the sample processed at 350 °C.

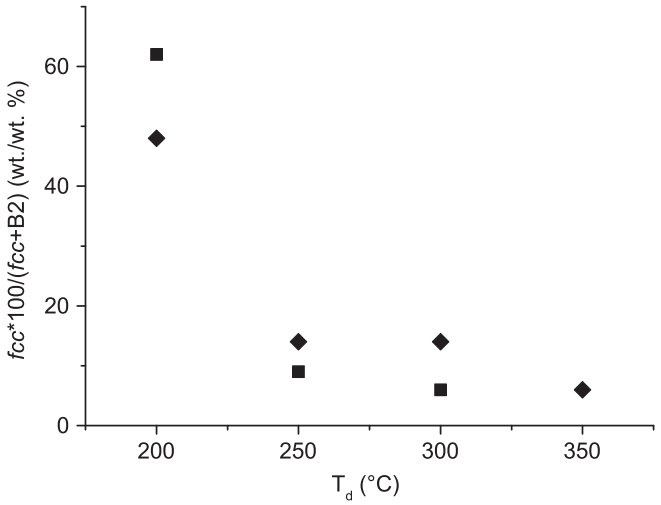

Fig. 4. *fcc* over the sum *fcc* plus B2 weight ratio of the Pd–Cu phases in the films as a function of T_d. Squares and diamonds correspond to films processed by thermal, and combined thermal and VUV activation, respectively.

As expected, XPS systematically revealed oxygen and carbon surface impurities. Determination of O concentration in the films is awkward due to the overlap of O1*s* and Pd3*p* peaks. However, the absence of intense O*KLL* lines in the Auger area shows that the oxygen concentration is low, if not negligible. Films are persistently C contaminated, at the level of 15 at% for those processed by thermal activation, and of 20 at% for those processed by combined thermal and VUV activation. C concentration hardly depends on T_d, except for 350 °C, where it slightly increases to attend 25 at% for films processed under VUV activation. Fig. 4 presents the *fcc* over the sum *fcc* plus B2 weight ratio of the Pd–Cu phases in the films as a function of T_d. It can be noticed that the *fcc* phase prevails at the lowest T_d; i.e. for films processed at 200 °C. In this temperature, the considered ratio exceeds 60% for films processed under thermal activation, and it reaches almost 50% for those processed under VUV assistance. For both type of films, this ratio strongly

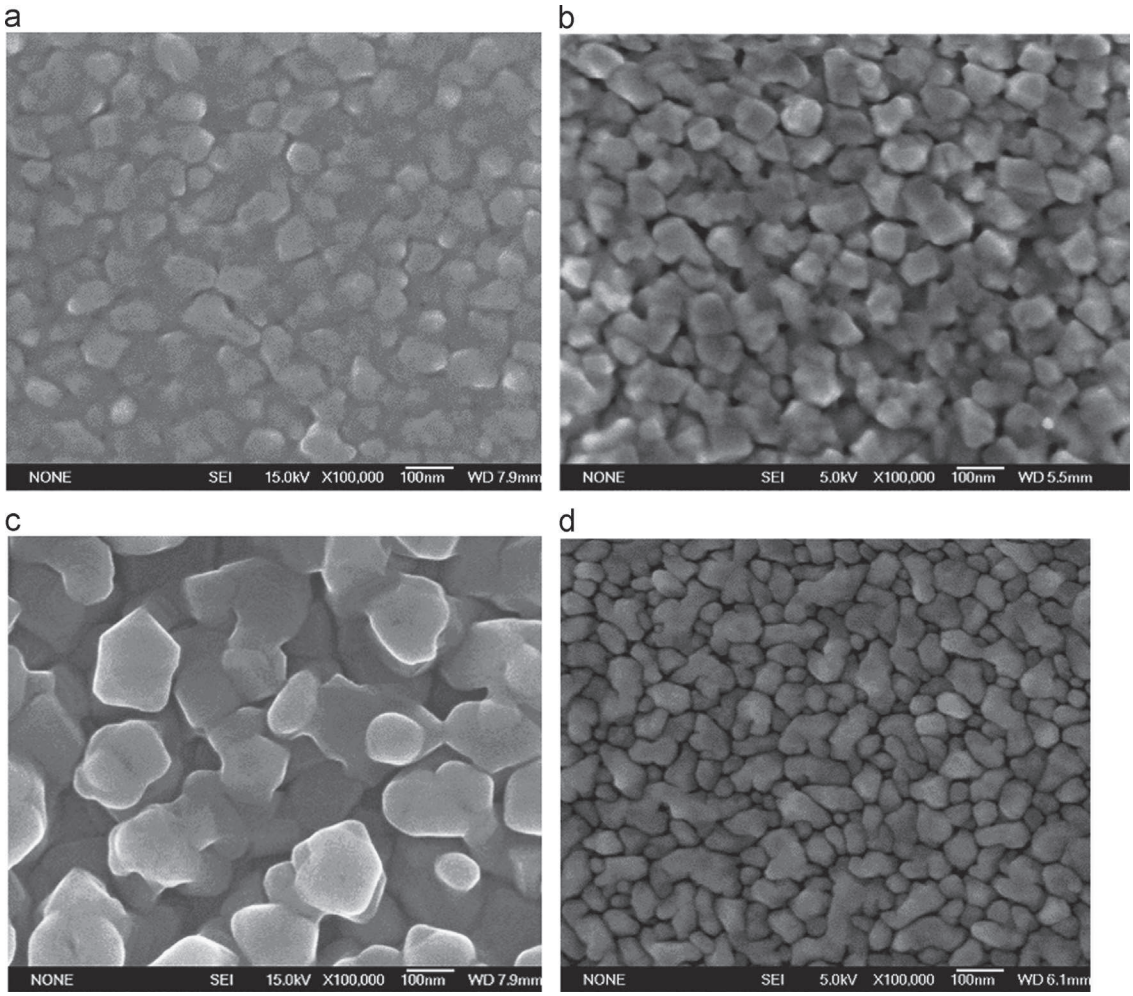

Fig. 5. SEM surface views for typical Pd–Cu alloy films prepared under thermal activation at T_d=250 °C (a) and 350 °C (c) and combined thermal plus VUV activation at T_d=250 °C (b) and 350 °C (d). Films are deposited on fused silica.

decreases with increasing T_d to reach 14% and 9% for films processed with and without VUV activation, respectively. Above this temperature it slightly decreases for both types of films.

Fig. 5 presents SEM surface views of four samples, processed at T_d=250 °C and 350 °C under thermal and combined thermal plus VUV activation. The estimated thickness of all films is between 200 nm and 300 nm. Films present a uniform microstructure, composed of grains which are facetted at T_d=250 °C independently of the activation mode. Grain size at this T_d is approximately 70–80 nm, slightly less for films grown under VUV. Increase of T_d to 350 °C results in round shaped grains whose size is *ca*. 150 nm for films grown under thermal activation. In contrast, the grain size of films grown at this T_d under VUV does not significantly increase. These films are more smoother and more compact; i.e. they present a reduced porosity than the thermally grown ones, independently of T_d.

4. Conclusion

A novel approach for the preparation of Pd-alloy membrane materials by CVD is demonstrated. Pd–Cu films were deposited from $PdL_2 \times CuL_2$, (L=2-methoxy-2,6,6-trimethylheptane-3,5-dionate), a new, non-toxic, halogen free single source bimetallic precursor with a 1:1 Cu/Pd ratio. Deposition conditions were 10 Torr, under thermal (temperature range 200–350 °C) and combined thermal and Vacuum Ultra Violet activation. Films of tunable composition and microstructure have been obtained in this parametric space. They are composed of the cubic B2 and the *fcc* Pd–Cu phases, with predominance of the former and significant content of the latter at low deposition temperature. Films are systematically Cu-rich, with a mean value of Cu/Pd ratio of 55/45. The morphology of the films is uniform and rough, with faceted grains for films deposited under thermal activation, the size of which increases from 70 to 80 nm at 250 °C to *ca*. 150 nm at 350 °C. These grains are composed of crystallites, whose size increases from 10 ± 5 nm at 200 °C to *ca*. 45 nm at 350 °C. VUV activation of the deposition results in higher growth rate and in a moderate increase of the carbon content of the films which passes from approximately 15 at% to 20 at% and even 25 at% at 350 °C. It also provides films with smoother morphology and a slightly higher content of the *fcc* phase in the temperature range 250–300 °C, namely *ca*. 17 wt% to be compared with 10 wt% and less for films deposited through thermal activation. Carbon impurities determination seems to be problematic and needs further verification.

Acknowledgments

The authors are grateful to Mrs. T.P. Koretskaya (Nikolaev Institute of Inorganic Chemistry SB RAS) for VUV-assisted experiments, Dr. N.I. Petrova and Dr. A.R. Tsygankova (Nikolaev Institute of Inorganic Chemistry SB RAS) for ISP-AES analysis, Dr. E.V. Maximovskiy (Nikolaev Institute of Inorganic Chemistry SB RAS) for operating SEM, and Dr. V.V. Kaichev (Boreskov Institute of Catalysis SB RAS) for the help with XPS analysis. The reported study was partially supported by RFBR, research Project no. 14-03-00411-a.

References

[1] F. Gallucci, A. Basile, F. Ibney Hai, Introduction – a review of membrane reactors, in: A. Basile, F. Gallucci (Eds.), Membranes for Membrane Reactors: Preparation, Optimization and Selection, John Wiley & Sons, United Kingdom, 2011, pp. 1–61.
[2] G.S. Burkhanov, N.B. Gorina, N.B. Kolchugina, N.R. Roshan, D.I. Slovetsky, E.M. Chistov, Platin. Met. Rev. 55 (1) (2011) 3–12.
[3] G.Q. Lu, J.C. Diniz da Costa, M. Duke, S. Giessler, R. Socolow, R.H. Williams, T. Kreutz, J. Colloid Interface Sci. 314 (2007) 589–603.
[4] P.M. Thoen, F. Roa, J.D. Way, Desalination 193 (2006) 224–229.
[5] C. Resini, L. Arrighi, M.C. Herrera Delgado, M.A. Larrubia Vargas, L.J. Alemany, P. Riani, S. Berardinelli, R. Marazza, G. Busca, Int. J. Hydrog. Energy 31 (2006) 13–19.
[6] F. Borgognoni, S. Tosti, M. Vadrucci, A. Santucci, Int. J. Hydrog. Energy 38 (2013) 1430–1438.
[7] S. Tosti, Int. J. Hydrog. Energy 35 (2010) 12650–12659.
[8] Y. She, S.C. Emerson, N.J. Magdefrau, S.M. Opalka, C. Thibaud-Erkey, T.H. Vanderspurt, J. Membr. Sci. 452 (2014) 203–211.
[9] S. Nayebossadri, J. Speight, D. Book, J. Membr. Sci. 451 (2014) 216–225.
[10] T.A. Peters, T. Kaleta, M. Stange, R. Bredesen, J. Membr. Sci. 383 (2011) 124–134.
[11] R.J. Gouwen, C.J.G.M. de Kok, J.A.Z. Pieterse, Noble Metal Membrane Preparation: Industrial Film Formation Techniques, CATO-2 Report # WP1.2.F1-D02.
[12] J. Prabhuram, T.S. Zhao, Z.X. Liang, H. Yang, C.W. Wong, J. Electrochem. Soc. 152 (7) (2005) A1390–A1397.
[13] M.Z.F. Kamarudin, S.K. Kamarudin, M.S. Masdar, W.R.W. Daud, Int. J. Hydrog. Energy 38 (2013) 9438–9453.
[14] K. Babita, S. Sridhar, K.V. Raghavan, Int. J. Hydrog. Energy 36 (2011) 6671–6688.
[15] E. Antolini, E.R. Gonzalez, J. Power Sources 195 (2010) 3431–3450.
[16] V. Bhaskaran, P. Atanasova, M.J. Hampden-Smith, T.T. Kodas, Chem. Mater. 9 (1997) 2822–2829.
[17] C.W. Park, R.W. Vook, Thin Solid Films 226 (1993) 238–241.
[18] C. Vahlas, Chemical vapor deposition of metals: from unary systems to complex metallic alloys, in: E. Belin-Ferré (Ed.), Complex Metallic Alloys: Surfaces and Coatings, World Scientific, Singapore, 2010, pp. 49–81.
[19] B.M. Kuchumov, T.P. Koretskaya, Y.V. Shevtsov, S.V. Trubin, G.I. Zharkova, V.S. Danilovich, I.K. Igumenov, V.N. Kruchinin, ECS Trans. 25 (8) (2009) 909–916.
[20] Powder Diffraction File, PDF-2/Release 2009, 2009: International Centre for Diffraction Date, USA.
[21] W. Kraus, G. Nolze, PowderCell 2.4, Program for the Representation and Manipulation of Crystal Structures and Calculation of the Resulting X-Ray Powder Patterns, Berlin, 2000.
[22] S. Krumm, Mater. Sci. Forum 183 (1996) 228–231.
[23] C.D. Wagner, W.M. Riggs, L.E. Davis, J.F. Moulder, Handbook of X-Ray Photoelectron Spectroscopy, in: G.E. Muilenberg (Ed.), Perkin-Elmer Corporation, Eden Prairie, Minnesota, USA, 1978.
[24] B. Predel, Cu–Pd (copper–palladium), in: O. Madelung (Ed.), SpringerMaterials–The Landolt-Börnstein Database ⟨http://www.springermaterials.com⟩, doi: 10.1007/10086090_1102.
[25] W. Huang, S.M. Opalka, D. Wang, T.B. Flanagan, Thermodynamic modelling of the Cu–Pd–H system, CALPHAD 31 (2007) 315–329.
[26] M. Hansen, K. Anderko, Constitution of Binary Alloys, Mc Graw-Hill, New York (1958) 1305.
[27] J. Batista, A. Pintar, D. Mandrino, M. Jenko, V. Martin, Appl. Catal. A. 206 (2001) 113–124.
[28] Thomas Christiansen, A.J. Somers, Marcel, stress and composition of carbon stabilized expanded austenite on stainless steel, Metall. Mater. Trans. A Phys. Metall. Mater. Sci. 40A (8) (2009) 1791–1798.
[29] V.I. Bukhtiyarov, V.V. Kaichev, I.P. Prosvirin, Top. Catal. 32 (2005) 3–15.
[30] N.S. McIntyre, M.G. Cook, Anal. Chem. 47 (1975) 2208–2213.
[31] J.C. Otamiri, S.L.T. Andersson, A. Andersson, Appl. Catal. 65 (1990) 159–174.
[32] S. Poulston, P.M. Parlett, P. Stone, M. Bowker, Surf. Interface Anal. 24 (1996) 811–820.
[33] M. Richter, M.J.G. Fait, R. Eckelt, M. Scneider, J. Radnik, D. Heidemann, R. Fricke, J. Catal. 245 (2007) 11–24.
[34] B.R. Strohmeier, D.E. Leyden, R.S. Field, D.M. Hercules, J. Catal. 94 (1985) 514–530.
[35] S.A. Khromova, A.A. Smirnov, O.A. Bulavchenko, A.A. Saraev, V.V. Kaichev, S.I. Reshetnikov, V.A. Yakovlev, Appl. Catal. A 470 (2014) 261–270.
[36] T. Yano, M. Ebizuka, S. Shibata, M. Yamane, J. Electron Spectrosc. Relat. Phenom. 131–132 (2003) 133–144.